Physiologic RNA Targets and Refined Sequence Specificity of Coronavirus EndoU

Ancar et al.

Supplemental Figures and Tables

SUPPLEMENTAL FIGURES AND TABLES

Figure S1. Frequency and location of endoribonuclease cleavage sites in U6 snRNA and MHV negative-strand RNA in WT, IFNAR$^{-/-}$, and RNase L$^{-/-}$ BMM. Normalized 2´-3´-cp cDNA reads captured at each position along the (A) U6 snRNA and (B) MHV negative-strand RNA at 9 and 12 hpi with MHV$^{(S)}$, MHV$^{(V)}$, PDE^{mut}, and EndoU^{mut} virus in IFNAR$^{-/-}$ BMM.

Figure S2. Frequency and location of endoribonuclease cleavage sites in MHV positive-strand RNA in IFNAR and RNase L KO BMM. (A and B) Normalized cyclic phosphate cDNA reads captured at each position along the MHV genomic RNA at 9 and 12 hpi with MHV$^{(S)}$, MHV$^{(V)}$, PDE^{mut}, and EndoU^{mut} virus in (A) IFNAR$^{-/-}$ and (B) RNase L$^{-/-}$ BMM. Putative cleavage sites attributed to EndoU or RNase L were calculated from RNase L- or EndoU-dependent signal generated by subtracting signal from each captured position that occurs in the absence of either enzyme (RNase L$^{-/-}$ BMM or during EndoU^{mut} infection). These data were then filtered for sites with reads representing at least 0.01 % of total reads in the library. At each of these positions, the $\log_2$ fold change in signal when either RNase L or EndoU were absent was calculated and sites with ≥ 2.5 fold change were designated putative RNase L or EndoU sites.

Figure S3. Dinucleotide cleavage pattern in MHV positive-strand RNA downstream of captured 3´ RNA end. Percent total 2´-3´-cp cDNA reads captured at each dinucleotide in WT BMM at 9 and 12 hpi for bases +1:+2 (A) and +2:+3 (B) from the captured cleavage position (0-base).

Figure S4. Endoribonuclease cleavage preferences in MHV RNA from IFNAR$^{-/-}$ and RNase L$^{-/-}$ BMM. (A) and (B) Dinucleotide specificity analysis for cleavage in MHV positive-strand RNA by percent total cyclic phosphate cDNA reads captured at each 3´-dinucleotide at 9 and 12 hpi in (A) IFNAR$^{-/-}$ BMM for positions -2:-1 and in (B) RNase L$^{-/-}$ BMM for positions -1:+1.

Figure S5. Interaction between RNase L and EndoU cleavage at UA sequences in MHV RNA. (A) UA cleavage scoring analysis. All UA sequences in the MHV positive-strand RNA with >= 30 cyclic phosphate counts in either the UA↓ or U↓A cleavage position were compared by calculating the ratio of normalized counts (UA↓ counts /U↓A counts). Ratios > 1 were scored as UA↓ (RNase L) sites and ratios <1 were scored as U↓A sites (EndoU) and total number of scored sites for either position are shown for each condition of viral infection in IFNAR$^{-/-}$ and RNase L$^{-/-}$ BMM. (B) Frequency and location of UA positions in WT BMM under all conditions of viral infection which had ≥ 50 counts at U↓A positions and ≤ 1 counts at UA↓ positions. The top 5 of these positions by normalized count are labeled. (C) Frequency and location of UA positions in IFNAR$^{-/-}$ and RNase L$^{-/-}$ BMM under all conditions of viral infection which had ≥ 50 counts at U↓A positions and ≤ 1 counts at UA↓ positions.

Figure S6. MHV RNA abundance and RNAseq reads across the MHV genome. (A) Total RNAseq normalized counts assigned to MHV genomic features for each library. (B) Coverage of RNAseq read density across the MHV genome in reads per million.

Figure S7. Frequency and location of endoribonuclease cleavage in MHV 3′-UTR. Nucleotide and sequence resolution graphs displaying normalized counts in (A) WT, (B) IFNAR$^{-/-}$ (C) RNase L$^{-/-}$ BMM during infection with MHV$^{(V)}$ and EndoU^{mut} MHV. Nucleotide resolution graphs of region directly upstream of poly-A tail with cyclic phosphate counts normalized by RNA abundance in (D) WT, (E) IFNAR$^{-/-}$ (F) RNase L$^{-/-}$ BMM.

Figure S8. Regional cleavage of MHV RNA and subgenomic mRNA abundance. A) Percent normalized cyclic phosphate signal captured per MHV genomic region and normalized to length of each region for WT, IFNAR$^{-/-}$, RNase L$^{-/-}$ BMM across all conditions of viral infection at 12 hpi. Dotted line represents baseline percent of cleavage expected by cell type ([total number of cyclic phosphate counts / total genome size x 100]). (B) Cyclic phosphate counts normalized by viral RNA abundance displayed by region for WT, IFNAR$^{-/-}$, RNase L$^{-/-}$ BMM across all

conditions of viral infection at 12 hpi. (C) Percent cyclic phosphate counts normalized by mRNA abundance and to the length of each region for WT, IFNAR$^{-/-}$, RNase L$^{-/-}$ BMM across all conditions of viral infection at 12 hpi.

Figure S9. Cyclic phosphate sequencing analysis of experiment 2. (A) Normalized cyclic phosphate cDNA reads ([reads at each position / total reads in library]) aligning to host and viral RNAs at 9 and 12 hpi in WT and RNase L$^{-/-}$ bone marrow macrophages (BMM). (B) Putative cleavage sites attributed to EndoU or RNase L were calculated from RNase L- or EndoU-dependent signal generated by subtracting signal from each captured position that occurs in the absence of either enzyme (RNase L$^{-/-}$ BMM or during EndoU^{mut} infection). These data were then filtered for sites with reads representing at least 0.01 % of total reads in the library. At each of these positions, the log2 fold change in signal when either RNase L or EndoU were absent was calculated and sites with >= 2.5 fold change were called as putative RNase L or EndoU sites. (C and D) Dinucleotide specificity analysis for cleavage in MHV positive-strand RNA by percent total cDNA reads captured at each 3´-dinucleotide in WT BMM at 9 and 12 hpi for (C) Dinucleotide analysis for positions -2: -1 and (D) Dinucleotide analysis for positions -1:+1 from captured cleavage position (0 position). (E) Cumulative distribution of normalized counts by position of the MHV genome for every position with >= 10 cyclic phosphates counts across all cell types and infection conditions. (F) UA cleavage scoring analysis. All UA sequences in the MHV positive-strand RNA with ≥ 30 cyclic phosphate counts in either the UA↓ or U↓A cleavage position were compared by calculating the ratio of normalized counts (UA↓ counts /U↓A counts). Ratios > 1 were scored as UA↓ (RNase L) sites and ratios <1 were scored as U↓A sites (EndoU) and total number of scored sites for either position are shown for each condition of viral infection in WT BMM at 9 and 12 hpi. (G) Nucleotide and sequence resolution graphs displaying normalized counts in WT BMM during infection with MHV$^{(S)}$ and EndoU^{mut} MHV of region directly upstream of poly(A) tail.

Figure S10. Cyclic phosphate and RNAseq analysis of MHV RNA from experiment 2. (A) Sum of normalized counts displayed by region for WT and RNase $L^{-/-}$ BMM across all conditions of viral infection at 12 hpi. Transcription regulatory sequences (TRS) are numbered by their associated mRNA (2-7). Other genomic regions are labeled as shown in Figure 1A. (B) Sum of cyclic phosphate counts normalized by mRNA abundance and length of each genomic region [(sum per region (cyclic phosphate counts / RNAseq counts) / length of region (bp) *100] sum of cyclic phosphate abundance normalized counts per region)/length of region * 100] displayed by region for WT and RNase $L^{-/-}$ BMM across all conditions of viral infection at 12 hpi. (C) Normalized counts (sum of subgenomic mRNA / sum of all mRNAs) of subgenomic mRNAs detected in WT and RNase $L^{-/-}$ BMM across all conditions of viral infection at 9 and 12 hpi.

Figure S11. Endoribonuclease cleavage of rRNA during WT and mutant MHV infection. (A) RNase L-dependent cleavage sites in 18S rRNA by fold change in signal when comparing WT or $IFNAR^{-/-}$ BMM mock-infected or infected with $MHV^{(S),}$ $MHV^{(V)}$, PDE^{mut}, and $EndoU^{mut}$ virus to RNase $L^{-/-}$ BMM. Log2 fold change in the absence of RNase L activity was calculated for each position in the rRNA. The distribution of the top 100 RNase L-dependent cleavage sites were compared in WT and $IFNAR^{-/-}$ BMM under conditions of mock infection or infection with $MHV^{(S),}$ $MHV^{(V)}$, PDE^{mut}, and $EndoU^{mut}$ virus at 9 hpi. 18S rRNA was cleaved in an RNase L-dependent manner at UU^{542}, UU^{543}, UU^{771} and UA^{772}. (B) RNase L-dependent cleavage of 18S rRNA at UU^{771} and UA^{772} at 9 and 12 hpi, predominantly in MHV PDE^{mut}- and $EndoU^{mut}$-infected WT BMM. (C) Top 3 RNase L-dependent cleavage sites in 18S rRNA by fold change (log2WT BMM / RNase $L^{-/-}$ BMM) for all conditions of infection at 9 and 12 hpi in WT BMM. (D) Table of total RNase L- or EndoU-dependent cleavage sites in 18S, 28S, 5.8S, and 5S rRNA. RNase L- or EndoU-dependent cleavage were determined by identifying the top 1% of enzyme-dependent signal with a > 4 fold change in signal in the absence of RNase L or EndoU that match the RNase L ("UA", "UU", "UG", "UC") or EndoU ("UA", "CA") sequence preferences.

Figure S12. Correlation between cyclic phosphate counts and viral RNA abundance. (A and B). Correlation between viral RNA abundance and 2´-3´-cp counts at each base captured in the MHV positive-strand RNA (all comparisons significant ($p < 10^{\wedge 50}$) for experiment 1 (A) and experiment 2 (B). (C and D) Distribution of sites in MHV by normalized cyclic phosphates counts for sense and antisense RNAs from experiment 1 (C) and experiment 2 (D) across all conditions of infection and cell types. Positions are only shown if there was > 1 read in either the sense and antisense RNA.

Figure S13. Effect of WT and mutant MHV infection on other cellular endoribonucleases. Expression (log10 normalized RNAseq counts) of (A) RNase A, (B) angiogenin, (C) RNaseT2A, and (D) RNase T2B transcripts.

Figure S14. Differential expression of host RNAs involved in innate and inflammatory pathways during MHV infection. (A) Results of differential expression analysis within samples comparing 9 and 12 hpi using only samples with at least 2 replicates. (B and C) Gene ontology (GO) analysis of host gene expression during MHV infection. Categories of biological processes (BP) enriched with significantly upregulated genes ($p < 0.01$, lo2FC > 2) during infection with (B) $MHV^{(s)}$ or (C) $EndoU^{mut}$ in WT BMM. All significantly enriched (weightFisher < 0.01) results from the BP category are shown. (D and E) Heatmaps showing the expression of transcripts from the enriched GO categories involving (D) “cytokine enrichment” and (E) “positive regulation of NF-kappaB” ordered by hierarchical clustering for experiments 1 and 2 at 12 hpi.

Figure S15. Relationship between cyclic phosphate and RNAseq abundance in host mRNAs. (A and B) An Enrichment score was calculated for mRNAs using the total sum of cyclic phosphate or RNAseq normalized counts in mock/wt MHV/PDE^{mut} samples / total sum of cyclic phosphate or RNAseq normalized counts in $EndoU^{mut}$ samples at 9 and 12 hpi in WT and RNase $L^{-/-}$ BMM (enrichment score = [sample] / [$EndoU^{mut}$]) for experiment 1 (A) and experiment 2 (B). Genes were assigned to bins as follows: Bin1 = cyclic phosphate and

RNAseq enrichment scores were < 1, Bin 2 = cyclic phosphate and RNAseq enrichment scores >=1, Bin 3 = cyclic phosphate score < 1 and RNAseq score > 1=, Bin 4 = cyclic phosphate score >= 1 and RNAseq score < 1. Each bin includes genes assigned from 9 and 12 hpi and highlighted genes include those identified as part of the dsRNA response (Fig. 7C) and those involved in innate and inflammatory signaling (Figs, 7D and 7E).

Figure S16. Endoribonuclease cleavage specificity of host mRNAs during MHV infection. (A-D) Dinucleotide specificity analysis for cleavage of transcripts involved in the dsRNA response (Fig. 7C) during infection with mock, $MHV^{(V)}$ and $EndoU^{mut}$ for positions -2:-1 (A) or mock, $MHV^{(V)}$ and PDE^{mut} for positions -1:+1 (B) from experiment 1. For experiment 2, analysis included mock, $MHV^{(s)}$, PDE^{mut}, and $EndoU^{mut}$ for positions -2:-1 (C) and positions -1:+1 (D) in WT and WT and RNase L $^{-/-}$ BMM. Percent of cleavage at each 3´-dinucleotide was calculated relative to the total cDNA reads aligned to the mm10 transcriptome per library at 9 and 12 hpi. (E and F) Dinucleotide specificity analysis for all mRNAs during infection with mock, $MHV^{(s)}$, $MHV^{(V)}$, PDE^{mut}, and $EndoU^{mut}$ viruses for positions -2:-1 (E) and positions -1:+1 (F) in WT BMM from experiment 1.

Table S1 and S2. Dinucleotide enrichment and de-enrichment analysis at 9 and 12 hpi in WT BMM. Complete tables of dinucleotide enrichment and de-enrichment for -2 base: +2 base (table 1) or -1 base:-1 base (table 2) from the captured RNA end (0-base position) for each condition of viral infection at 9 and 12 hpi in WT BMM by comparing the frequency of dinucleotide capture in experimental conditions to the frequency of occurrence for each dinucleotide in the MHV genomic RNA sequence (control). Significant enrichment was determined by adjusted p-value (q) for fold change (log2(experiment / control)). ($<0.02^{*}$, $<0.0001^{**}$, $<1x10^{8***}$).

Table S3: SNP variants in MHV genome related to endoribonuclease cleavage. Table of all single nucleotide variants (SNPs) identify from alignments of RNAseq libraries to the MHV

genome. The SNPs in **green** are sites where the mutation generated a “CA” dinucleotide that was cleaved by EndoU. The SNPs in **red** and **yellow** are the inactivating mutations in the EndoU and PDE domains of MHV respectively.

Table S4: Coronavirus RNA sequences adjacent to poly(A) tail.

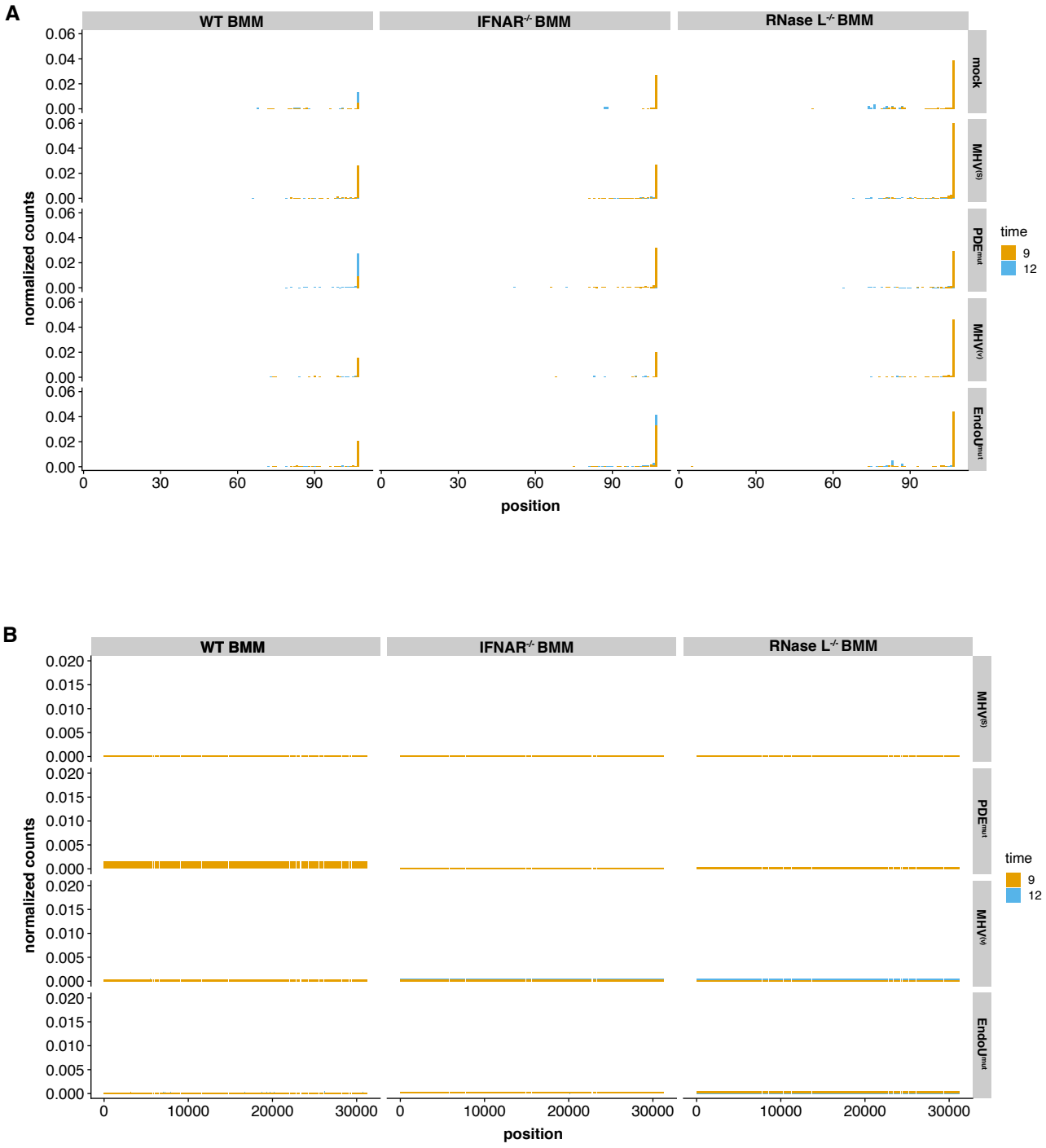
A
WT BMM
IFNAR-/- BMM
RNase L-/- BMM
mock
MHV(S)
PDEmut
MHV(V)
EndoUmut
normalized counts
0.06
0.04
0.02
0.00
0
30
60
90
position
time
9
12

B
WT BMM
IFNAR-/- BMM
RNase L-/- BMM
MHV(S)
PDEmut
MHV(V)
EndoUmut
normalized counts
0.020
0.015
0.010
0.005
0.000
0
10000
20000
30000
position
time
9
12

Figure S1

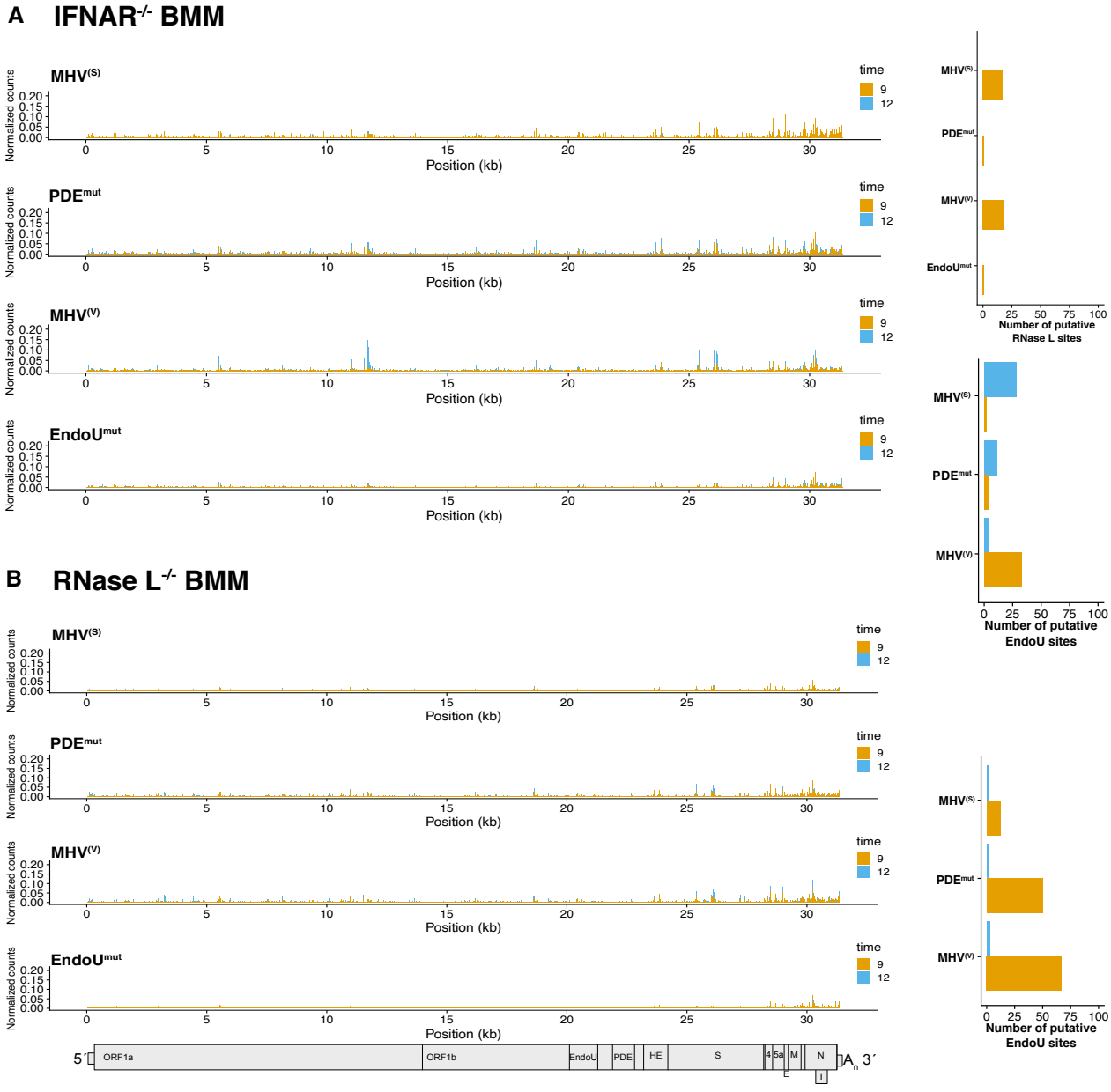
A IFNAR-/- BMM
MHV(S)
PDEmut
MHV(V)
EndoUmut
Normalized counts
Position (kb)
time
9
12
Number of putative RNase L sites
B RNase L-/- BMM
Number of putative EndoU sites
5′
ORF1a
ORF1b
EndoU
PDE
HE
S
4
5a
M
N
E
I
An 3′

Figure S2

A **Position +1 to +2 dinucleotide analysis in WT BMM**

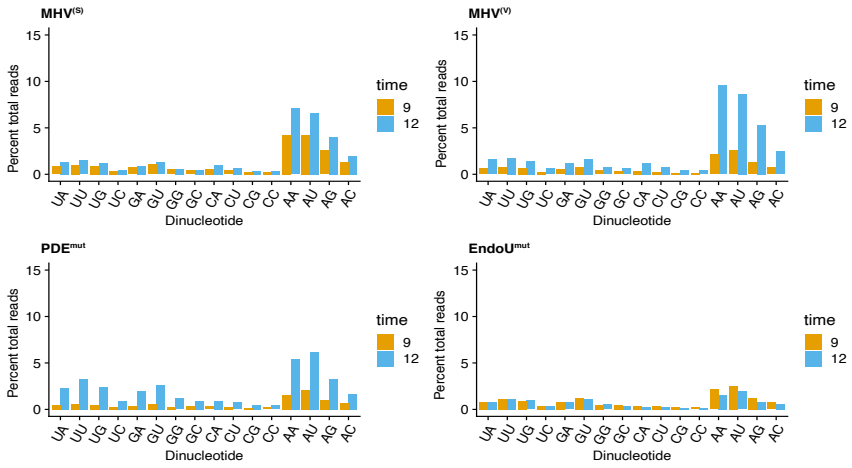

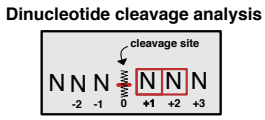

B **Position +2 to +3 dinucleotide analysis in WT BMM**

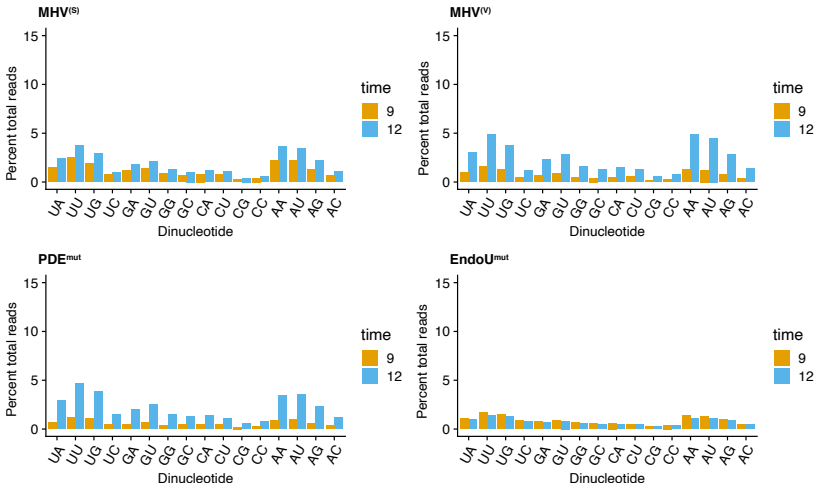

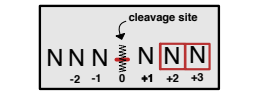

Figure S3

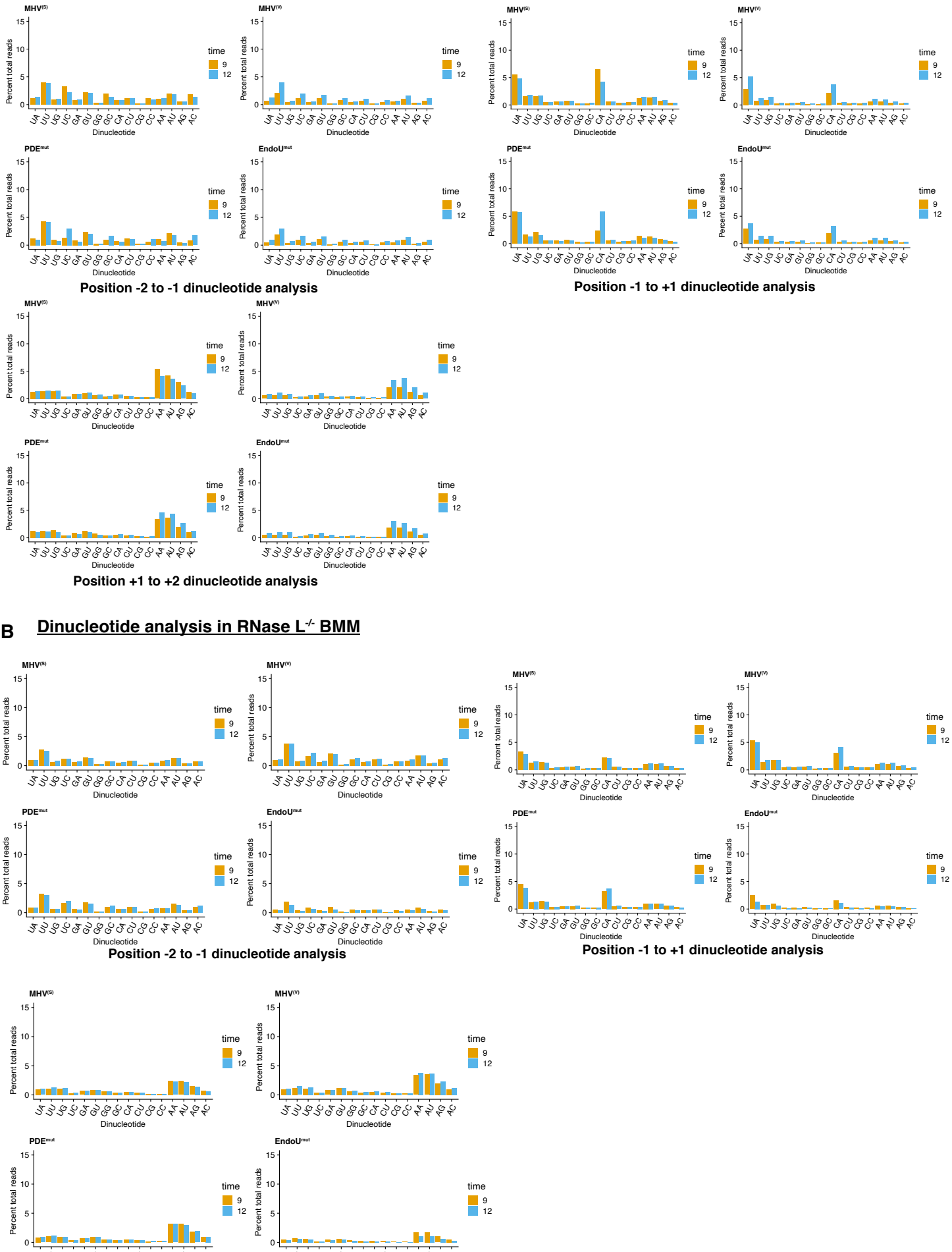
A
Dinucleotide analysis in IFNAR-/- BMM
MHV(S)
MHV(V)
PDEmut
EndoUmut
Percent total reads
Dinucleotide
time
9
12
Position -2 to -1 dinucleotide analysis
Position -1 to +1 dinucleotide analysis
Position +1 to +2 dinucleotide analysis
B
Dinucleotide analysis in RNase L-/- BMM
Position -2 to -1 dinucleotide analysis
Position -1 to +1 dinucleotide analysis
Position +1 to +2 dinucleotide analysis

Figure S4

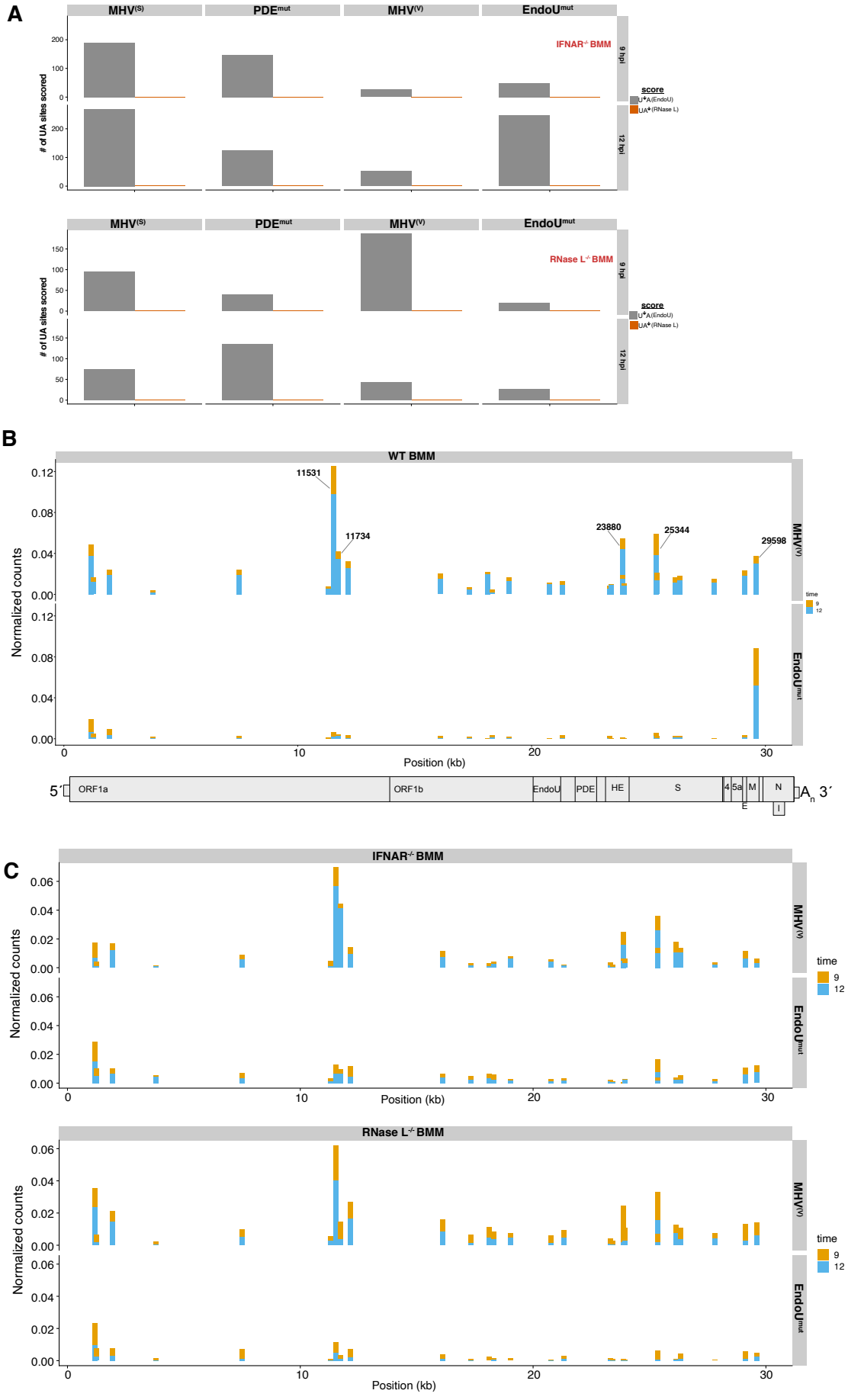
A
MHV(S)
PDEmut
MHV(V)
EndoUmut
IFNAR-/- BMM
RNase L-/- BMM
# of UA sites scored
9 hpi
12 hpi
score
U*A(EndoU)
UA*(RNase L)
B
WT BMM
Normalized counts
Position (kb)
11531
11734
23880
25344
29598
time
5´
ORF1a
ORF1b
EndoU
PDE
HE
S
4
5a
M
N
E
I
An 3´
C
IFNAR-/- BMM
RNase L-/- BMM

Figure S5

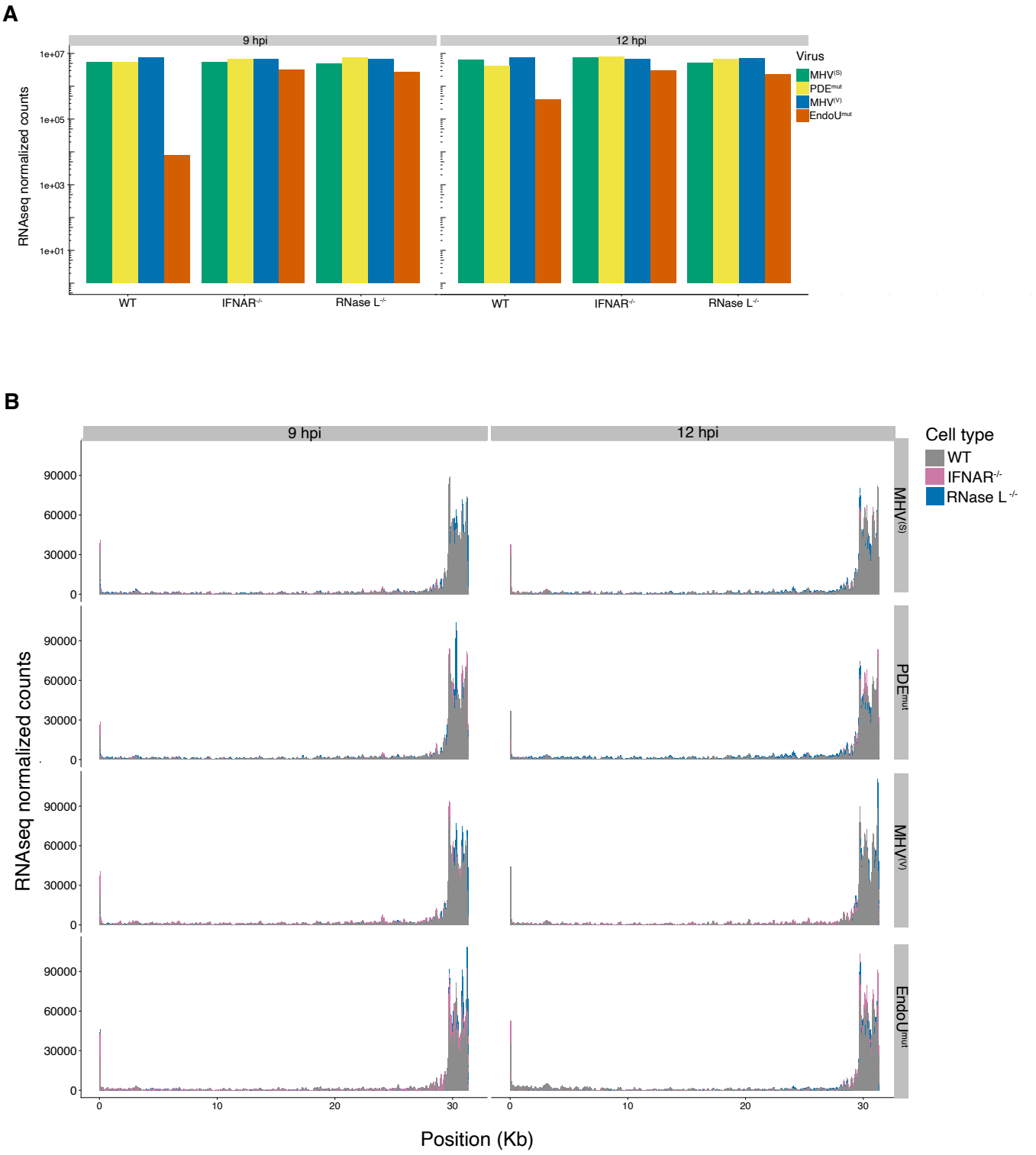
A
9 hpi
12 hpi
RNAseq normalized counts
1e+07
1e+05
1e+03
1e+01
WT
IFNAR-/-
RNase L-/-
Virus
MHV(S)
PDEmut
MHV(V)
EndoUmut
B
Cell type
WT
IFNAR-/-
RNase L-/-
MHV(S)
PDEmut
MHV(V)
EndoUmut
90000
60000
30000
0
10
20
30
Position (Kb)

Figure S6

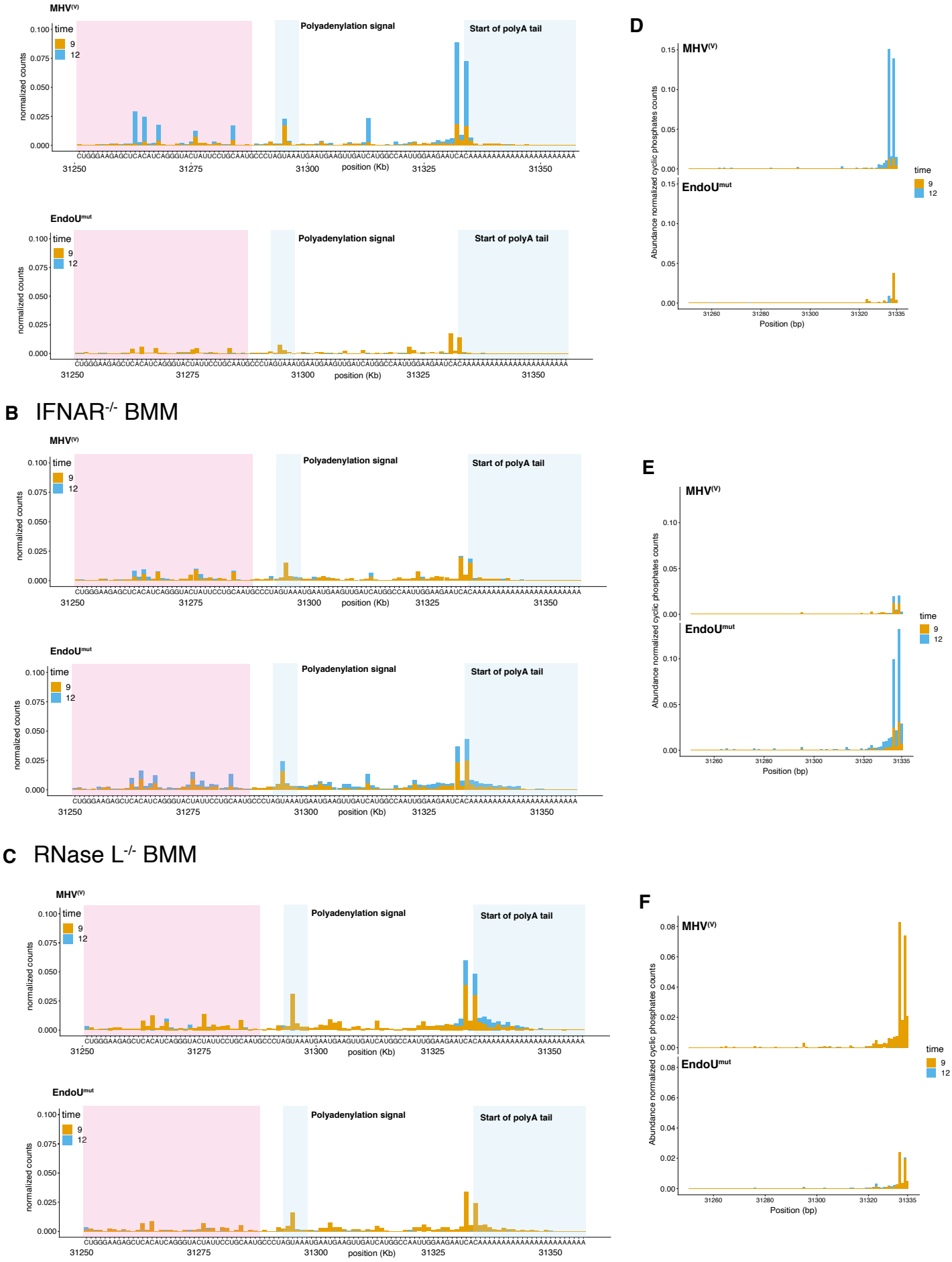
A WT BMM
MHV(V)
Polyadenylation signal
Start of polyA tail
time
9
12
normalized counts
position (Kb)
EndoUmut
B IFNAR-/- BMM
C RNase L-/- BMM
D
E
F
Abundance normalized cyclic phosphates counts
Position (bp)

Figure S7

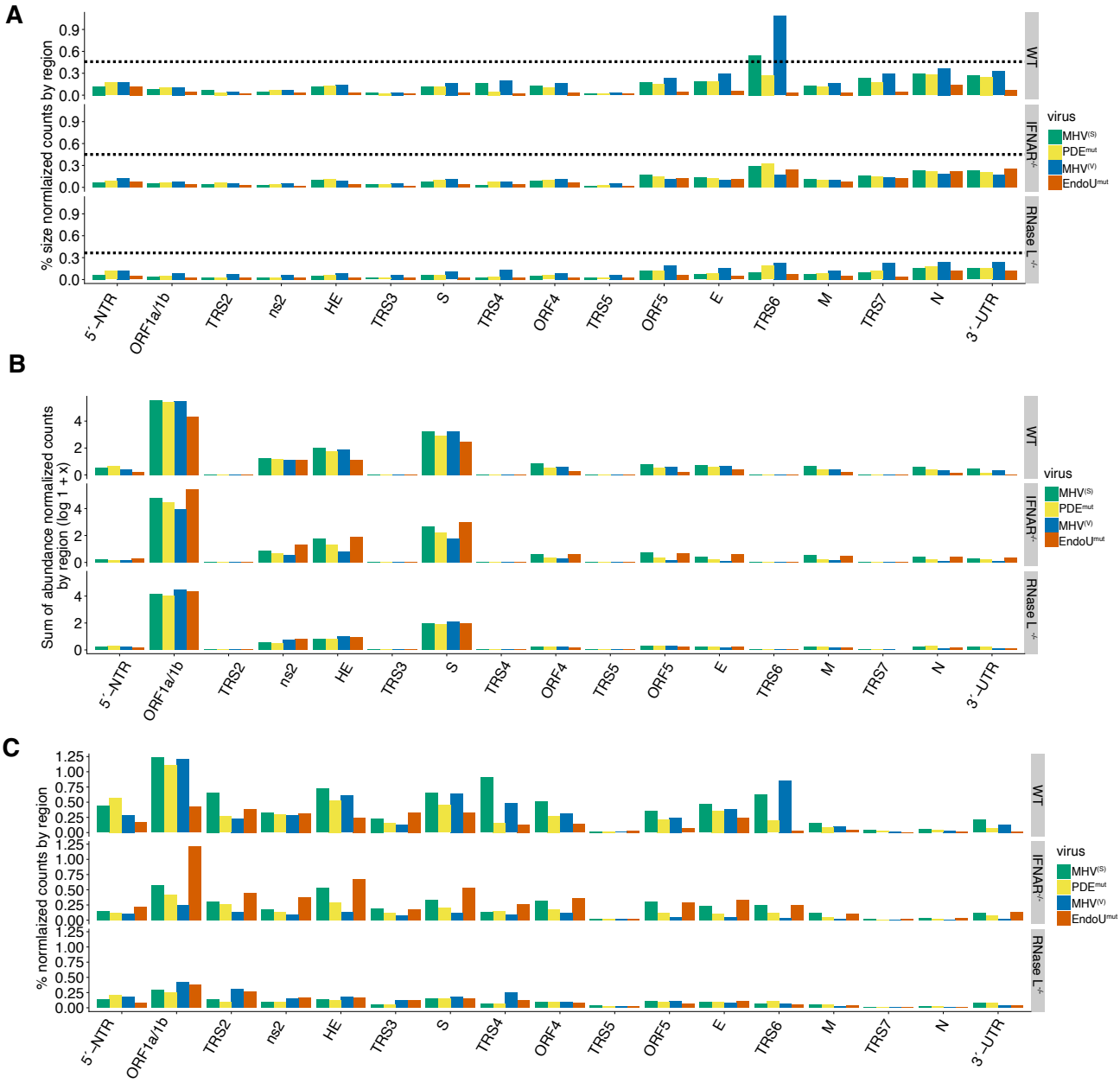
A
% size normlaized counts by region
WT
IFNAR-/-
RNase L-/-
virus
MHV(S)
PDEmut
MHV(V)
EndoUmut
5´-NTR
ORF1a/1b
TRS2
ns2
HE
TRS3
S
TRS4
ORF4
TRS5
ORF5
E
TRS6
M
TRS7
N
3´-UTR
B
Sum of abundance normalized counts by region (log 1 + x)
C
% normlaized counts by region

Figure S8

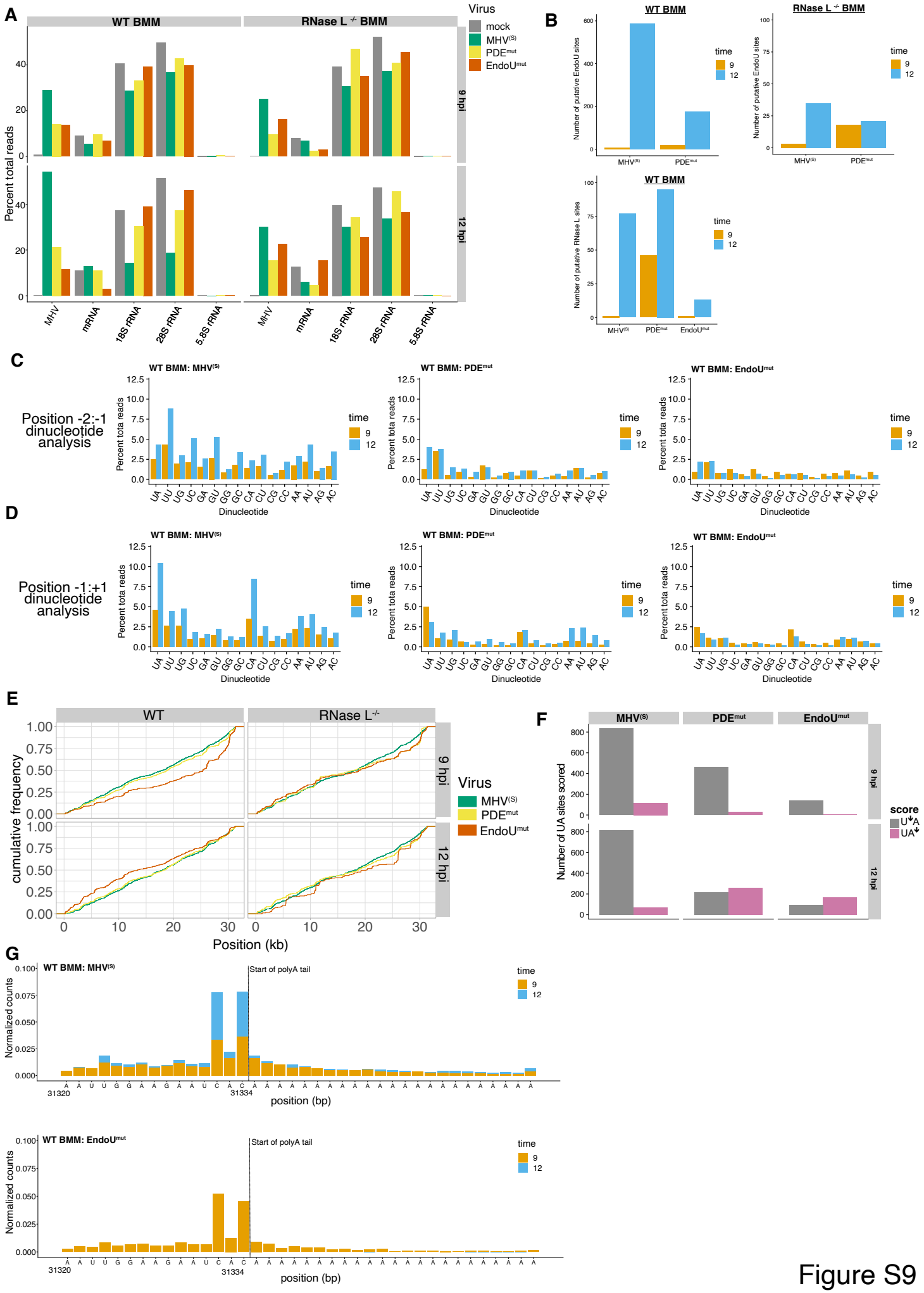
A
WT BMM
RNase L -/- BMM
Virus
mock
MHV(S)
PDEmut
EndoUmut
Percent total reads
9 hpi
12 hpi
MHV
mRNA
18S rRNA
28S rRNA
5.8S rRNA
B
WT BMM
RNase L -/- BMM
Number of putative EndoU sites
Number of putative RNase L sites
time
9
12
C
Position -2:-1 dinucleotide analysis
WT BMM: MHV(S)
WT BMM: PDEmut
WT BMM: EndoUmut
Percent tota reads
Dinucleotide
D
Position -1:+1 dinucleotide analysis
E
WT
RNase L-/-
cumulative frequency
Position (kb)
F
Number of UA sites scored
score
U↓A
UA↓
G
Normalized counts
Start of polyA tail
position (bp)

Figure S9

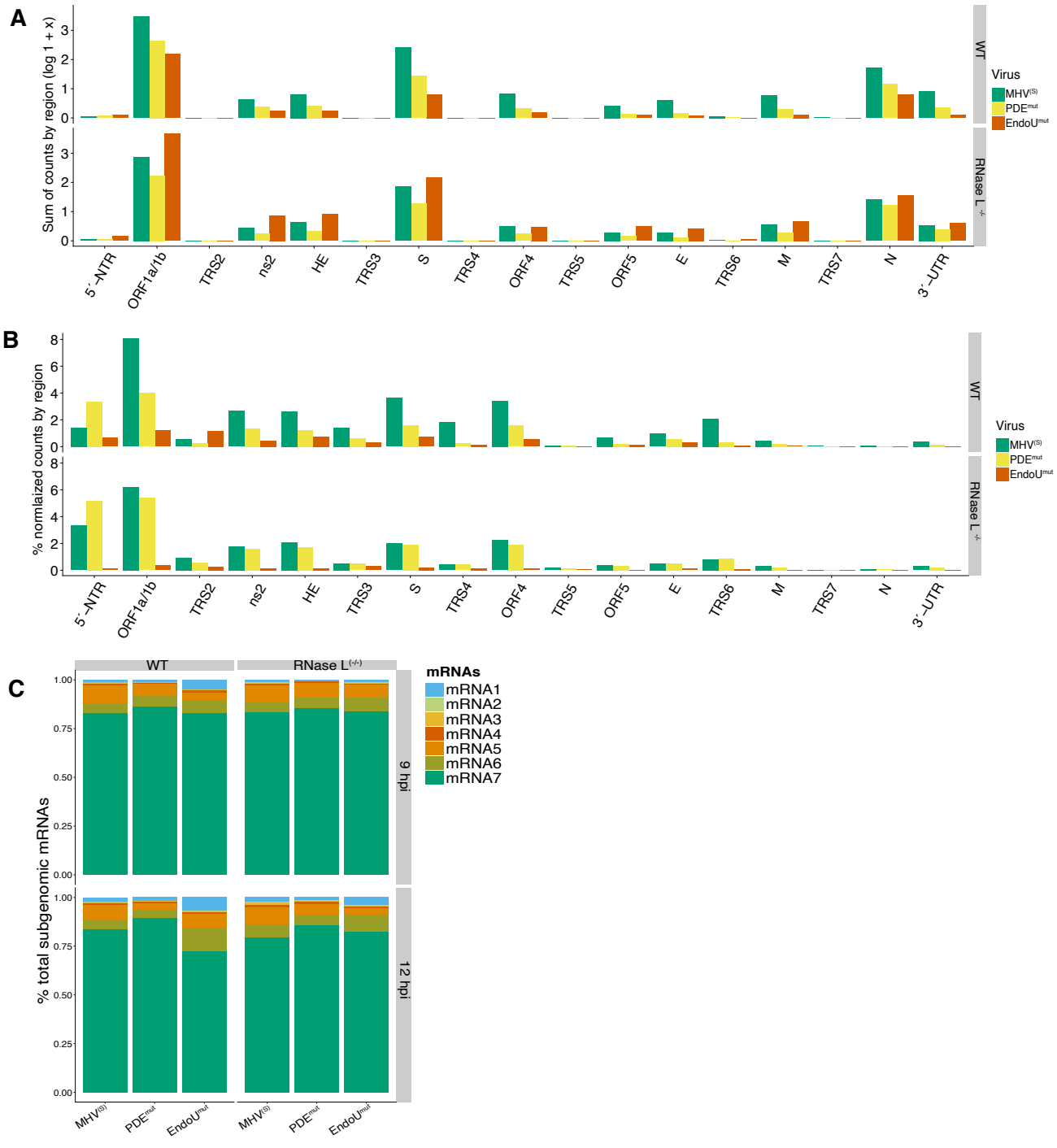
A
Sum of counts by region (log 1 + x)
WT
RNase L -/-
Virus
MHV(S)
PDEmut
EndoUmut
5´-NTR
ORF1a/1b
TRS2
ns2
HE
TRS3
S
TRS4
ORF4
TRS5
ORF5
E
TRS6
M
TRS7
N
3´-UTR
B
% normlaized counts by region
C
WT
RNase L(-/-)
mRNAs
mRNA1
mRNA2
mRNA3
mRNA4
mRNA5
mRNA6
mRNA7
9 hpi
12 hpi
% total subgenomic mRNAs
MHV(S)
PDEmut
EndoUmut

Figure S10

A

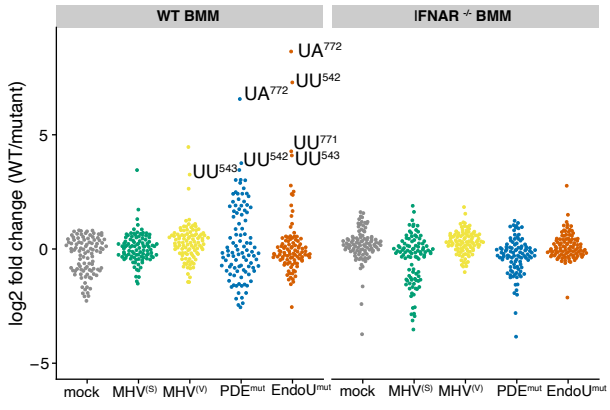

B

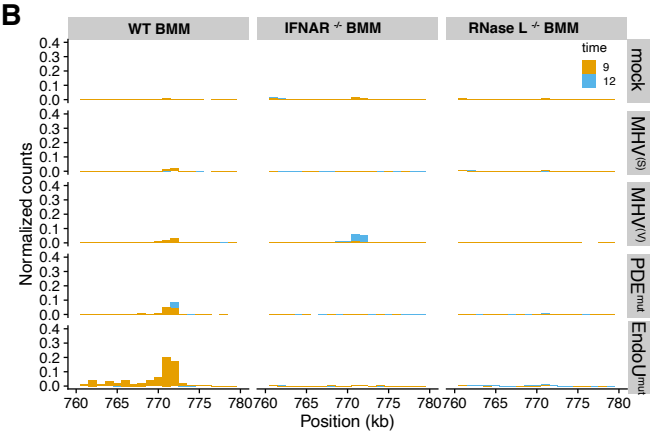

C

Position	time	mock	MHV$^{(S)}$	MHV$^{(V)}$	PDE^{mt}	EndoU^{mt}
UA^{772}	9	-1.09	3.47	4.48	6.58	8.66
UU^{771}	9	-0.65	1.32	2.65	3.77	7.30
UU^{543}	9	-2.05	-0.07	1.00	1.94	4.29
UA^{772}	12	2.21	3.29	1.02	5.52	4.88
UU^{542}	12	4.32	2.01	2.17	3.37	4.26
UU^{771}	12	-0.64	-0.33	1.55	1.57	3.94

D

	RNase L sites	EndoU sites
18S rRNA	8	0
28S rRNA	26	0
5.8S rRNA	3	0
5S rRNA	1	0

Figure S11

A

Cell	Virus	Corr. estimate
WT	MHV$^{(S)}$	0.151
WT	MHV$^{(V)}$	0.109
WT	PDE^{mut}	0.084
WT	EndoU^{mut}	0.139
IFNAR $^{-/-}$	MHV$^{(S)}$	0.194
IFNAR $^{-/-}$	MHV$^{(V)}$	0.103
IFNAR $^{-/-}$	PDE^{mut}	0.154
IFNAR $^{-/-}$	EndoU^{mut}	0.252
RNaseL $^{-/-}$	MHV$^{(S)}$	0.210
RNaseL $^{-/-}$	MHV$^{(V)}$	0.172
RNaseL $^{-/-}$	PDE^{mut}	0.174
RNaseL $^{-/-}$	EndoU^{mut}	0.229

B

Cell	Virus	Corr. estimate
WT	MHV$^{(S)}$	0.151
WT	PDE^{mut}	0.084
WT	EndoU^{mut}	0.139
RNaseL $^{-/-}$	MHV$^{(S)}$	0.194
RNaseL $^{-/-}$	PDE^{mut}	0.103
RNaseL $^{-/-}$	EndoU^{mut}	0.154

C

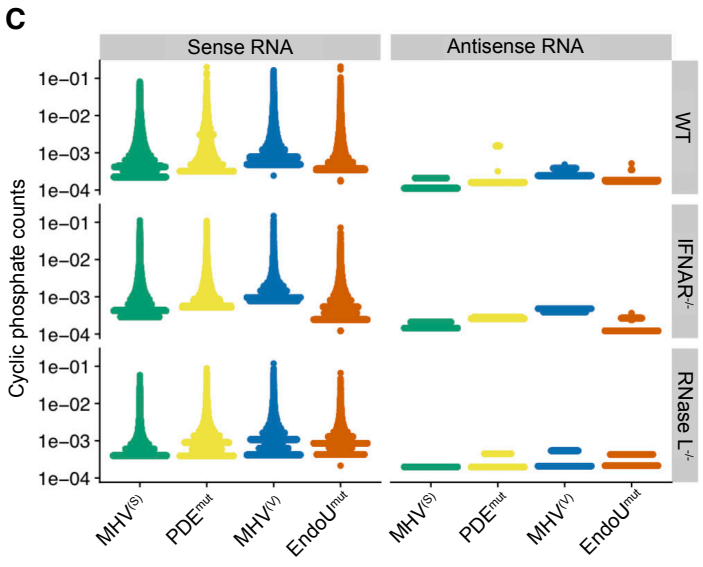

D

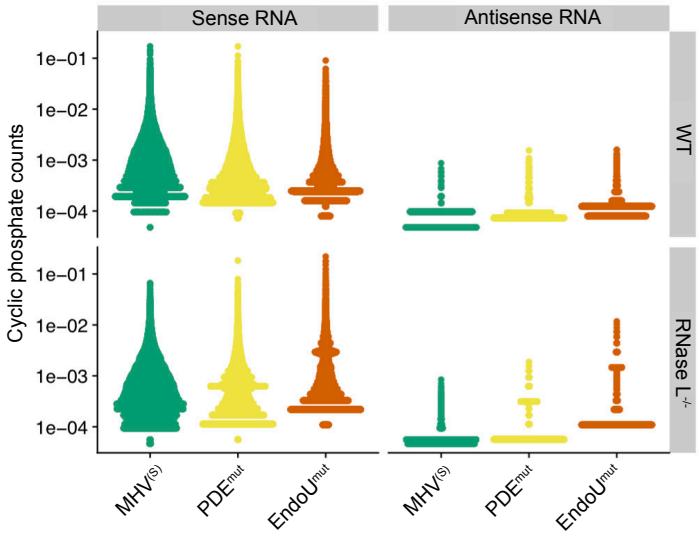

Figure S12

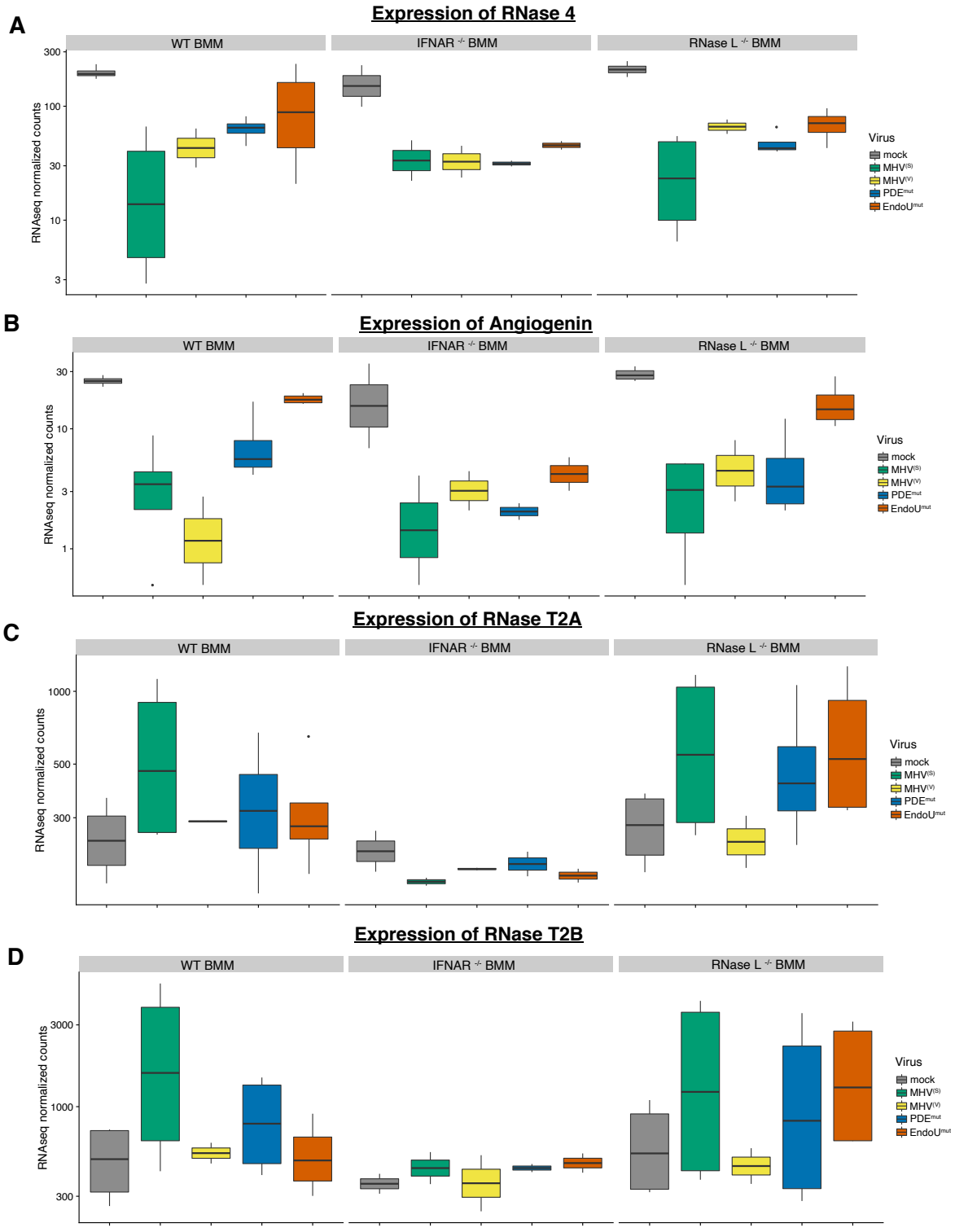
A
Expression of RNase 4
WT BMM
IFNAR -/- BMM
RNase L -/- BMM
RNAseq normalized counts
300
100
30
10
3
Virus
mock
MHV(S)
MHV(V)
PDEmut
EndoUmut
B
Expression of Angiogenin
WT BMM
IFNAR -/- BMM
RNase L -/- BMM
RNAseq normalized counts
30
10
3
1
Virus
mock
MHV(S)
MHV(V)
PDEmut
EndoUmut
C
Expression of RNase T2A
WT BMM
IFNAR -/- BMM
RNase L -/- BMM
RNAseq normalized counts
1000
500
300
Virus
mock
MHV(S)
MHV(V)
PDEmut
EndoUmut
D
Expression of RNase T2B
WT BMM
IFNAR -/- BMM
RNase L -/- BMM
RNAseq normalized counts
3000
1000
300
Virus
mock
MHV(S)
MHV(V)
PDEmut
EndoUmut

Figure S13

A

Differentially expressed genes within samples at 9 vs. 12 hpi

Cell type	Virus	Upregulated genes	Downregulated genes
WT	mock	0	1
WT	MHV$^{(S)}$	0	0
WT	MHV$^{(V)}$	2	2
WT	PDE^{mut}	0	0
WT	EndoU^{mut}	1	0
RNase L KO	mock	1	0
RNase L KO	MHV$^{(S)}$	0	1
RNase L KO	MHV$^{(V)}$	1	2
RNase L KO	PDE^{mut}	0	2
RNase L KO	EndoU^{mut}	0	0

B **GO terms in Biological Process: MHV$^{(s)}$ vs. Mock in WT BMM**

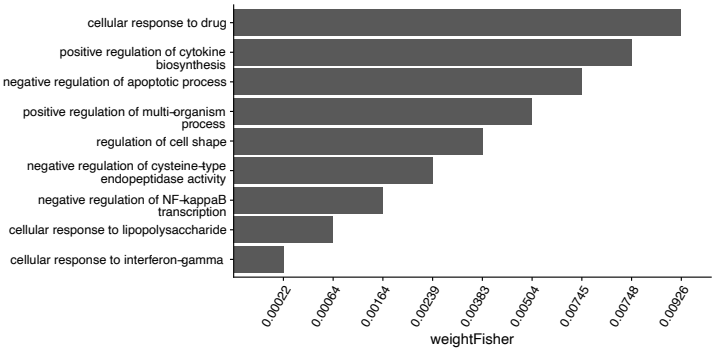

C

Top 5 GO terms in Biological Process: EndoU^{mut} vs. Mock in WT BMM

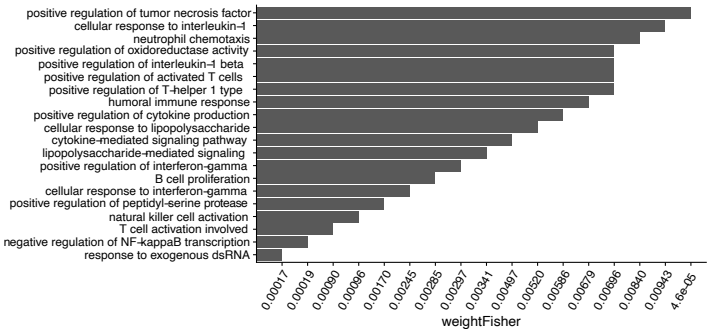

D

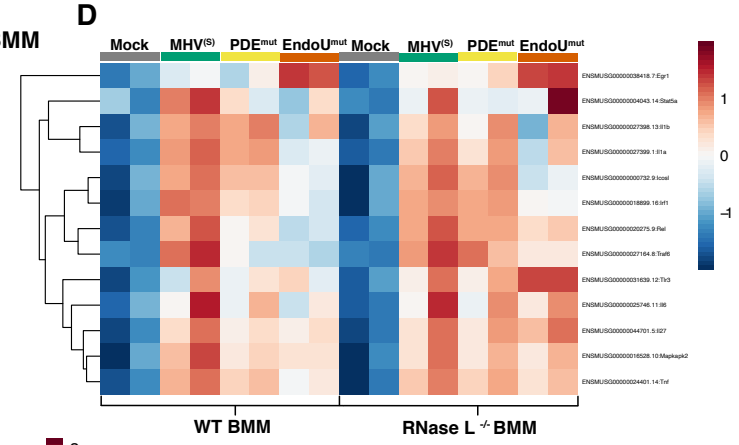

E

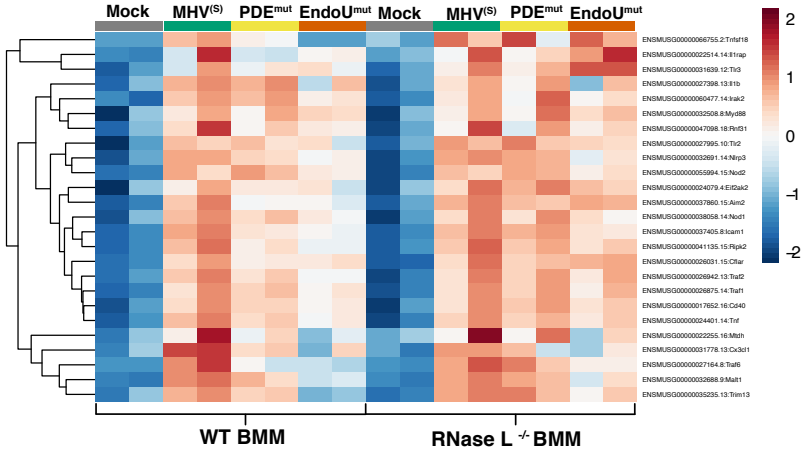

Figure S14

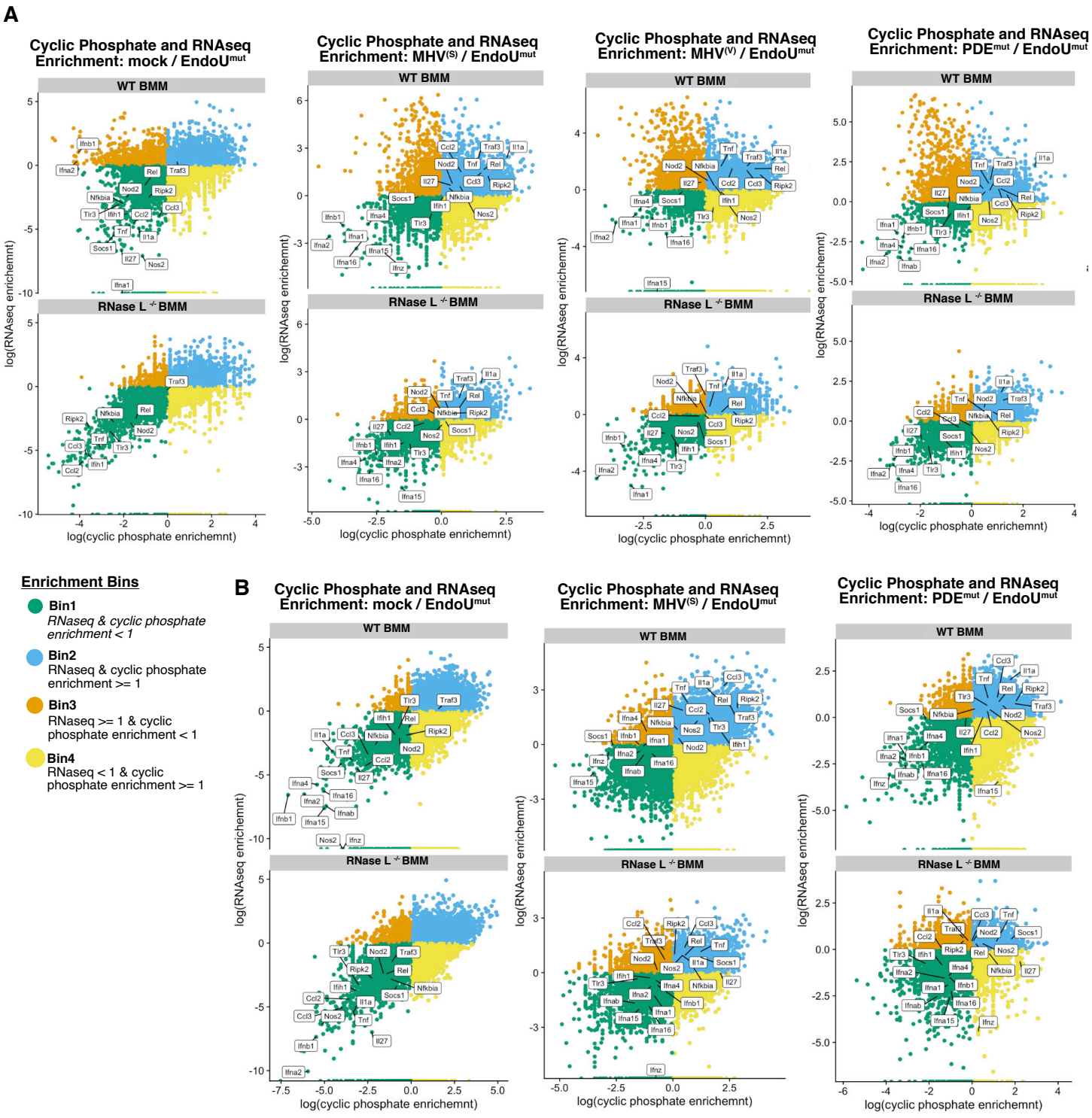
A
Cyclic Phosphate and RNAseq Enrichment: mock / EndoU^mut
Cyclic Phosphate and RNAseq Enrichment: MHV^(S) / EndoU^mut
Cyclic Phosphate and RNAseq Enrichment: MHV^(V) / EndoU^mut
Cyclic Phosphate and RNAseq Enrichment: PDE^mut / EndoU^mut
WT BMM
RNase L -/- BMM
log(RNAseq enrichemnt)
log(cyclic phosphate enrichemnt)
Enrichment Bins
Bin1
RNaseq & cyclic phosphate enrichment < 1
Bin2
RNaseq & cyclic phosphate enrichment >= 1
Bin3
RNaseq >= 1 & cyclic phosphate enrichment < 1
Bin4
RNaseq < 1 & cyclic phosphate enrichment >= 1
B
Cyclic Phosphate and RNAseq Enrichment: mock / EndoU^mut
Cyclic Phosphate and RNAseq Enrichment: MHV^(S) / EndoU^mut
Cyclic Phosphate and RNAseq Enrichment: PDE^mut / EndoU^mut

Figure S15


A
B
C
D
E
F
WT mock
RNase L -/- mock
WT MHV(V)
RNase L -/- MHV(V)
WT EndoUmut
RNase L -/-EndoUmut
WT MHV(S)
RNase L -/- MHV(S)
WT PDEmut
RNase L -/-PDEmut
Percent total reads
Percent total umi-reads
Dinucleotide
time
9
12

Figure S16

Table 1A. Dinucleotide enrichment and de-enrichment in WT BMM at 12 hpi(position -2 to -1)

	MHV$^{(S)}$		MHV$^{(V)}$		PDE^{mut}		EndoU^{mut}	
Dinucleotide	Fold change	qval	Fold change	qval	Fold change	qval	Fold change	qval
UA	-0.57	1	-0.59	1	1.36	0.0E-1000	1.71	0.0E-1000
UU	1.01	0.0E-1000	0.97	0.0E-1000	1.22	0.0E-1000	1.35	0.0E-1000
UG	-1.87	1	-1.98	1	-0.69	1	-0.29	1
UC	1.80	0.0E-1000	1.99	0.0E-1000	0.87	4.81E-123	0.15	0.0018
GA	-1.65	1	-1.79	1	-1.24	1	-1.05	1
GU	0.29	1.19E-23	0.15	6.35E-07	-0.23	1	-0.94	1
GG	-2.67	1	-2.83	1	-2.65	1	-2.70	1
GC	0.69	5.32E-99	0.78	1.22E-120	-0.30	1	-1.01	1
CA	-0.89	1	-1.00	1	-0.42	1	0.20	6.52E-07
CU	-0.11	1	-0.27	1	-0.55	1	-0.88	1
CG	-1.94	1	-2.05	1	-1.98	1	-1.86	1
CC	0.52	3.96E-38	0.62	4.42E-52	-0.45	1	-1.03	1
AA	-1.60	1	-1.77	1	-1.01	1	-0.74	1
AU	0.10	0.0005	0.00	1	-0.34	1	-0.90	1
AG	-2.20	1	-2.44	1	-2.11	1	-2.08	1
AC	0.98	3.21E-174	1.11	7.50E-221	0.10	0.0195	-0.61	1

Table 1B. Dinucleotide enrichment and de-enrichment in WT BMM at 9 hpi(position -2 to -1)

	MHV$^{(S)}$		MHV$^{(V)}$		PDE^{mut}		EndoU^{mut}	
Dinucleotide	Fold change	qval	Fold change	qval	Fold change	qval	Fold change	qval
UA	-0.20	1	0.13	0.00135	0.19	0.0071	1.43	0.0E-1000
UU	1.04	0.0E-1000	1.21	0.0E-1000	0.94	9.92E-88	1.27	0.0E-1000
UG	-1.71	1	-1.43	1	-1.21	1	-0.45	1
UC	1.57	0.0E-1000	0.92	4.41E-84	0.70	8.77E-17	0.68	5.39E-59
GA	-1.22	1	-0.94	1	-0.88	1	-1.03	1
GU	0.41	4.91E-41	0.50	8.87E-43	0.65	2.73E-27	-0.60	1
GG	-2.46	1	-2.11	1	-1.51	1	-2.78	1
GC	0.50	1.95E-41	0.01	0.981	0.26	0.00181	-0.41	1
CA	-0.71	1	-0.53	1	-0.15	1	0.21	2.18E-07
CU	-0.03	1	0.08	0.111	0.29	0.00019	-0.81	1
CG	-1.72	1	-1.40	1	-1.27	1	-1.93	1
CC	0.29	1.19E-10	-0.11	1	-0.09	1	-0.49	1
AA	-1.22	1	-0.89	1	-0.98	1	-0.77	1
AU	0.12	0.00019	0.31	2.33E-16	0.32	6.74E-07	-0.79	1
AG	-1.95	1	-1.76	1	-1.97	1	-2.28	1
AC	0.66	6.51E-63	0.17	0.0014	-0.03	1	-0.12	1

Table 2A. Dinucleotide enrichment and de-enrichment in WT BMM at 12 hpi(position -1 to +1)

	MHV$^{(S)}$		MHV$^{(V)}$		PDE^{mut}		EndoU^{mut}	
Dinucleotide	Fold change	qval	Fold change	qval	Fold change	qval	Fold change	qval
UA	2.00	0.0E-1000	1.93	0.0E-1000	1.43	0.0E-1000	1.02	1.05E-281
UU	-0.85	1	-1.06	1	-0.19	1	-0.18	1
UG	-0.82	1	-0.79	1	-0.06	1	0.15	3.42E-07
UC	-0.67	1	-0.94	1	-0.99	1	-0.84	1
GA	-1.94	1	-2.03	1	-1.17	1	-0.93	1
GU	-1.81	1	-1.97	1	-1.04	1	-0.84	1
GG	-2.60	1	-2.75	1	-1.44	1	-0.85	1
GC	-2.39	1	-2.59	1	-2.50	1	-2.34	1
CA	2.46	0.0E-1000	2.60	0.0E-1000	1.40	0.0E-1000	0.56	8.72E-50
CU	-1.01	1	-0.95	1	-1.31	1	-1.57	1
CG	-0.58	1	-0.28	1	-1.00	1	-1.38	1
CC	-0.49	1	-0.35	1	-1.32	1	-1.82	1
AA	-0.83	1	-0.89	1	0.51	1.78E-68	0.98	2.08E-239
AU	-0.88	1	-1.00	1	0.37	3.80E-39	0.62	5.98E-95
AG	-1.36	1	-1.44	1	0.04	0.670003	0.41	8.99E-31
AC	-1.64	1	-1.73	1	-0.72	1	-0.37	1

Table 2B. Dinucleotide enrichment and de-enrichment in WT BMM at 9 hpi(position -1 to -1)

	MHV$^{(S)}$		MHV$^{(V)}$		PDE^{mut}		EndoU^{mut}	
Dinucleotide	Fold change	qval	Fold change	qval	Fold change	qval	Fold change	qval
UA	2.01	0.0E-1000	2.06	0.0E-1000	2.08	0.0E-1000	1.28	0.0E-1000
UU	-0.91	1	-0.52	1	-0.76	1	-0.46	1
UG	-0.41	1	-0.04	1	-0.28	1	-0.02	1
UC	-0.72	1	-0.79	1	-0.59	1	-0.84	1
GA	-1.61	1	-1.27	1	-1.59	1	-1.05	1
GU	-1.70	1	-1.48	1	-1.24	1	-1.10	1
GG	-2.24	1	-2.00	1	-1.73	1	-1.00	1
GC	-2.36	1	-2.03	1	-1.38	1	-2.23	1
CA	2.18	0.0E-1000	1.49	0.0E-1000	1.38	3.23E-112	1.24	2.27E-302
CU	-1.11	1	-1.17	1	-0.97	1	-1.61	1
CG	-0.41	1	-0.35	1	-0.42	1	-0.96	1
CC	-0.70	1	-0.98	1	-0.90	1	-1.40	1
AA	-0.35	1	-0.06	1	0.03	1	0.86	3.03E-182
AU	-0.69	1	-0.40	1	-0.42	1	0.32	2.80E-24
AG	-0.99	1	-0.66	1	-0.59	1	0.27	1.19E-13
AC	-1.40	1	-1.15	1	-0.65	1	-0.45	1

Position (bp)	Reference	Variant
67	T	C
256	A	T
2471	T	C
5304	T	C
6265	C	T
6796	A	T
7475	G	A
9245	C	T
10136	A	C
12140	G	A
13604	G	A
16624	G	C
16990	C	T
17533	T	G
18646	**A**	**C**
18681	C	T
20552	**C**	**G**
20553	**A**	**C**
20554	**T**	**G**
22147	**A**	**G**
22739	T	G
22742	T	C
23393	C	T
23860	T	C
24404	T	A
24447	G	A
24448	C	T
24450	T	A
26074	G	C
28960	**T**	**C**
29012	G	C
29650	T	C

Table S3

Genus	Virus	3’ NTR / poly(A) junction	Accession #
Alpha CoVs	HCoV NL63	auggauacacaaaaa	AY567487
	HCoV 229E	auggauacacaaaaa	AF304460
Beta CoVs	MHV A59	gaagaaucacaaaaa	NC_001846.1
	HCoV OC43	gaagaaucacaaaaa	NC_006213.1
	HCoV HKU1	gaggaauuacaaaaa	AY597011
	MERS-CoV	gaugauuugcaaaaa	KJ556336.1
	SARS-CoV	ggagaaugacaaaaa	AY274119.3
	SARS-CoV-2	ggagaaugacaaaaa	MN908947.3
	Bat CoV HKU9	gaggauuugcaaaaa	MG762674.1
Gamma CoVs	IBV	gaguuagagcaaaaa	MN987231.1
	Beluga Whale CoV	aauuguuagcaaaaa	NC_010646.1
Delta CoVs	Porcine CoV HKU15	gggauggagcaaaaa	KJ569769.1
	Bulbul CoV HKU11	gggagggagcaaaaa	NC_011547.1

Table S4